

Spin-polarized tunneling in the half-metallic ferromagnets $\text{La}_{0.7-x}\text{Ho}_x\text{Sr}_{0.3}\text{MnO}_3$ ($x = 0$ and 0.15): Experiment and theory

P. Raychaudhuri,^{*} K. Sheshadri, P. Taneja, S. Bandyopadhyay,[†]
 P. Ayyub, A. K. Nigam, and R. Pinto

Tata Institute of Fundamental Research, Homi Bhabha Road, Mumbai 400005, India

Sujeet Chaudhary and S. B. Roy

Centre for Advanced Technology, Indore-452013, India

(Received 13 July 1998; revised manuscript received 3 March 1999)

The magnetoresistance (MR) in polycrystalline colossal magnetoresistive compounds follows a behavior different from single crystals below the ferromagnetic transition temperature. This difference is usually attributed to spin-polarized tunneling at the grain boundaries of the polycrystalline sample. Here we derive a theoretical expression for the contribution of spin-polarized tunneling to the magnetoresistance in granular ferromagnetic systems under the mean-field approximation. We apply this model to our experimental data on two half-metallic ferromagnets, $\text{La}_{0.7}\text{Sr}_{0.3}\text{MnO}_3$ and $\text{La}_{0.55}\text{Ho}_{0.15}\text{Sr}_{0.3}\text{MnO}_3$ in the temperature range 5–300 K. We find that the theoretical predictions agree quite well with the observed dependence of the spin polarized MR on the spontaneous magnetization. We discuss the significance of our results in the light of the recent finding by A. Biswas *et al.* [Phys. Rev. B **59**, 5368 (1999)] regarding the evolution of the total density of states at the Fermi level as a function of temperature in colossal magnetoresistive materials.
 [S0163-1829(99)04405-7]

I. INTRODUCTION

The large amount of recent activity on colossal magnetoresistive (CMR) manganites has revived interest in the study of electrical transport in granular itinerant ferromagnets. Many of these materials (e.g., $\text{La}_{0.7}\text{Sr}_{0.3}\text{MnO}_3$, CrO_2 , Fe_3O_4) in the polycrystalline form are now known to exhibit large magnetoresistance at low fields below the ferromagnetic transition temperature (T_c).¹⁻⁴ Under similar conditions, magnetoresistance in single crystals is either very low or totally absent. The origin of this nonintrinsic intergranular effect is interesting and its detailed understanding should be important from a technological point of view.

Though several researchers have attributed this effect to intergranular spin polarized tunneling,^{1,5-7} a complete understanding of this phenomenon is lacking. Comparing the magnetoresistance of single-crystalline and polycrystalline samples of $\text{La}_{0.7}\text{Sr}_{0.3}\text{MnO}_3$, Hwang *et al.*¹ suggested that spin-polarized tunneling at the polycrystalline grain boundaries might play a crucial role in determining the magnetotransport properties below the ferromagnetic T_c . They suggested that the magnetoresistance in polycrystalline $\text{La}_{0.7}\text{Sr}_{0.3}\text{MnO}_3$ originates from the following two sources: (i) an intrinsic part arising from Zener double exchange mechanism⁸ between two neighboring manganese ions, and (ii) the intergranular spin-polarized tunneling. The second component produces a sharp drop in resistance at low fields and is dominant at temperatures much below T_c , whereas the first component is dominant close to T_c . In an earlier paper⁶ we have shown that the intergranular part in the magnetoresistance can be distinguished from the intrinsic part by considering the field dependence of the magnetoresistance. The contribution from the intergranular spin-polarized tun-

neling gives rise to a sharp drop in resistance at low fields and low temperatures. At high fields, the resistance varies almost linearly with the field. The high-field behavior can be attributed to the intrinsic Zener double exchange mechanism and explains the observations in single crystals. Thus one can estimate the resistance drop due to spin-polarized tunneling by finding the intercept obtained by extrapolating back the linear high-field region. Using this scheme, we had earlier shown that the intergranular magnetoresistance due to spin-polarized tunneling in polycrystalline colossal magnetoresistive manganites drops monotonically with temperature, whereas the intrinsic part follows the behavior expected from Zener double exchange.⁶

In an attempt to understand the mechanism of magnetoresistance in granular ferromagnets, Helman and Abeles⁹ had proposed a model based on intergranular spin-polarized tunneling. This model assumed that when an electron tunnels across a boundary between two grains having antiparallel magnetization, it will experience a potential barrier of the order of the exchange energy (E_m). So the tunneling probability between the two grains with antiparallel magnetization was assumed to be reduced by a factor $e^{-E_m/kT}$ from that when they are parallel. The conceptual difficulty in Helman and Abeles' model is the following. When the conduction band in the ferromagnet is partially polarized, the dominant factor guiding the tunneling probability is the respective up and down density of states (DOS) in the two grains. Inoue and Maekawa¹⁰ had pointed out the difficulty in taking an exponential factor in which the energy is of the order of exchange energy. Thus, the mechanism of spin-polarized transport in granular ferromagnets needs to be investigated in greater detail.

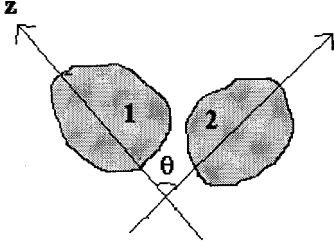


FIG. 1. Two neighboring ferromagnetic grains with magnetization \mathbf{M}_1 and \mathbf{M}_2 making an angle θ with respect to each other. In a sufficiently large applied field, θ becomes zero, thus increasing the tunneling probability of an electron from grain 1 to grain 2. In our convention, the z axis is along the magnetization direction of grain 1.

In this paper, we propose a model to understand the mechanism of spin-polarized tunneling in granular ferromagnets. Section II describes the theoretical model, while the sample preparation and experimental procedures are given in Sec. III. In Sec. IV, we compare the predictions of the theoretical model with the temperature and field dependence of spin-polarized tunneling in $\text{La}_{0.7}\text{Sr}_{0.3}\text{MnO}_3$ ($T_c \sim 370$ K) and $\text{La}_{0.55}\text{Ho}_{0.15}\text{Sr}_{0.3}\text{MnO}_3$ ($T_c \sim 255$ K). We also discuss the applicability of this model to other granular ferromagnets.

II. THEORETICAL MODEL

In a granular ferromagnet in zero field, the magnetization directions of the grains are randomly oriented due to the random orientation of their magnetocrystalline anisotropy axes. Following Inoue and Maekawa,¹⁰ we first derive an expression for the difference in the spin-polarized tunneling resistance between a configuration where the magnetization of two grains are at an angle θ , and that in which their magnetizations are made mutually parallel by the application of a magnetic field. Let n_\uparrow and n_\downarrow be the respective densities of states of up and down spins at the Fermi level. We choose our z axis to be parallel to the magnetization direction of grain 1 (see Fig. 1). The up- and down-spin eigenstates are defined as $|S_z; \uparrow\rangle = \begin{pmatrix} 1 \\ 0 \end{pmatrix}$ and $|S_z; \downarrow\rangle = \begin{pmatrix} 0 \\ 1 \end{pmatrix}$, respectively. We define the spin eigenstates in grain 2 as $|S_\theta; \uparrow\rangle$ and $|S_\theta; \downarrow\rangle$. Using the Pauli rotation matrix $R(\theta)$, we can easily find the relation between $|S_\theta; \uparrow\downarrow\rangle$ and $|S_z; \uparrow\downarrow\rangle$ from

$$|S_\theta; \uparrow\downarrow\rangle = R(\theta)|S_z; \uparrow\downarrow\rangle, \quad (1)$$

$$\text{where } R(\theta) = \begin{pmatrix} \cos(\theta/2) & -\sin(\theta/2) \\ \sin(\theta/2) & \cos(\theta/2) \end{pmatrix}.$$

Hence, we obtain

$$\begin{aligned} |S_\theta; \uparrow\rangle &= \cos(\theta/2)|S_z; \uparrow\rangle + \sin(\theta/2)|S_z; \downarrow\rangle, \\ |S_\theta; \downarrow\rangle &= -\sin(\theta/2)|S_z; \uparrow\rangle + \cos(\theta/2)|S_z; \downarrow\rangle. \end{aligned} \quad (2)$$

An electron can tunnel from grain 1 to grain 2 using one of the following channels:

- (a) $|S_z; \uparrow\rangle \rightarrow |S_\theta; \uparrow\rangle$,
- (b) $|S_z; \uparrow\rangle \rightarrow |S_\theta; \downarrow\rangle$,

$$(c) \quad |S_z; \downarrow\rangle \rightarrow |S_\theta; \uparrow\rangle,$$

$$(d) \quad |S_z; \downarrow\rangle \rightarrow |S_\theta; \downarrow\rangle.$$

Since the Hamiltonian involved with the tunneling process is spin independent, the matrix elements corresponding to (a) and (d) should be proportional to $\cos^2(\theta/2)$, and the matrix element corresponding to (b) and (c) should be proportional to $\sin^2(\theta/2)$. The total transition probability of up (or down) spin for tunneling from grain 1 to grain 2 should also depend on the initial and final DOS available to it in the two grains. Thus, the total transition probabilities for the four processes will be

$$T_a \propto n_\uparrow^2 \cos^2(\theta/2),$$

$$T_b \propto n_\uparrow n_\downarrow \sin^2(\theta/2),$$

$$T_c \propto n_\uparrow n_\downarrow \sin^2(\theta/2),$$

$$T_d \propto n_\downarrow^2 \cos^2(\theta/2).$$

The tunneling conductivity, $\sigma(\theta)$, between the two grains at angle θ involve the sum of all four processes. Thus,

$$\sigma(\theta) \propto (n_\uparrow^2 + n_\downarrow^2) \cos^2(\theta/2) + 2n_\uparrow n_\downarrow \sin^2(\theta/2)$$

or

$$\sigma(\theta) \propto (1/2)(n_\uparrow + n_\downarrow)^2 [1 + P^2 \cos\theta], \quad (3)$$

where $P = (n_\uparrow - n_\downarrow)/(n_\uparrow + n_\downarrow)$. When the magnetizations of grain 1 and grain 2 are made parallel to each other by applying a magnetic field, the conductivity becomes

$$\sigma(\theta=0) \propto (n_\uparrow^2 + n_\downarrow^2). \quad (4)$$

In a real system with many grains and grain boundaries one has to average over $\cos\theta$. Thus, the resistance change (ΔR_{spt}) arising due to spin-polarized tunneling is proportional to $[1/\sigma(\theta) - 1/\sigma(0)]$. One important point to note is the prefactor $(n_\uparrow + n_\downarrow)^2$ in Eq. (3). ΔR_{spt} is thus inversely proportional to the square of the total spin (spin up+spin down) density of states at the Fermi level (E_F) apart from its dependence on P , the polarization of the conduction band. As we shall show later, this can have very important implications if the density of states at E_F vary with temperature.

In order to determine the temperature dependence of ΔR_{spt} , we require the temperature dependence of n_\uparrow and n_\downarrow . We use the ferromagnetic Kondo Hamiltonian proposed for this system by Furukawa¹¹⁻¹³ to calculate the up and down DOS.

$$H = -t \sum_{\langle i,j \rangle} c_{i\sigma}^\dagger c_{j\sigma} - J_H \sum_i \sigma_i \cdot \mathbf{s}_i, \quad (5)$$

where t is the nearest-neighbor hopping energy of the e_g electrons and J_H is the local ferromagnetic Hund's rule coupling between the e_g electron spin \mathbf{s}_i and the t_{2g} spin σ_i at the i th site. In terms of $\sigma^\pm = \sigma^x \pm i\sigma^y$, σ^z , $\mathbf{s}^\pm = s^x \pm is^y$ we can write

$$H = -t \sum_{\langle i,j \rangle} c_{i\sigma}^\dagger c_{j\sigma} - \frac{J_H}{2} \sum_i (\sigma_i^+ s_i^- + \sigma_i^- s_i^+ + 2\sigma_i^z s_i^z). \quad (6)$$

We resort to a mean-field approximation in which the t_{2g} spin σ is treated as a classical vector, i.e., the operators σ^+ and σ^z are replaced by c numbers:

$$\sigma_i^- \equiv A, \quad \sigma_i^+ \equiv A^*, \quad \text{and} \quad \sigma_i^z \equiv B.$$

We also write the e_g spin operators in terms of annihilation and creation operators:

$$s_i^+ = c_{i\uparrow}^\dagger c_{i\downarrow}, \quad s_i^- = c_{i\downarrow}^\dagger c_{i\uparrow}, \quad \text{and} \quad s_i^z = \frac{1}{2}(c_{i\uparrow}^\dagger c_{i\uparrow} - c_{i\downarrow}^\dagger c_{i\downarrow}).$$

As a result, we get the following expression for the mean-field Hamiltonian:

$$H^{\text{MF}} = -t \sum_{\langle i,j \rangle} c_{i\sigma}^\dagger c_{j\sigma} - \frac{J_H}{2} \sum_i [A c_{i\uparrow}^\dagger c_{i\downarrow} + A^* c_{i\downarrow}^\dagger c_{i\uparrow} + B(c_{i\uparrow}^\dagger c_{i\uparrow} - c_{i\downarrow}^\dagger c_{i\downarrow})]. \quad (7)$$

Going over to \mathbf{k} space by Fourier transforming according to

$$c_{i\sigma}^\dagger = \sum_{\mathbf{k}} c_{\mathbf{k}\sigma}^\dagger e^{i\mathbf{k}\cdot\mathbf{r}} \quad (8)$$

we get

$$H^{\text{MF}} = \sum_{\mathbf{k}} \left[\left(-\gamma_{\mathbf{k}} - \frac{1}{2} B J_H \right) c_{\mathbf{k}\uparrow}^\dagger c_{\mathbf{k}\uparrow} + \left(-\gamma_{\mathbf{k}} + \frac{1}{2} B J_H \right) c_{\mathbf{k}\downarrow}^\dagger c_{\mathbf{k}\downarrow} - \frac{J_H}{2} (A c_{\mathbf{k}\uparrow}^\dagger c_{\mathbf{k}\downarrow} + A^* c_{\mathbf{k}\downarrow}^\dagger c_{\mathbf{k}\uparrow}) \right]. \quad (9)$$

Here $\gamma_{\mathbf{k}} = t \sum_{\Delta} e^{i\mathbf{k}\cdot\Delta}$ where Δ is the nearest-neighbor vector. We can rewrite this as

$$H^{\text{MF}} = \sum_{\mathbf{k}} (c_{\mathbf{k}\uparrow}^\dagger c_{\mathbf{k}\downarrow}^\dagger) h_{\mathbf{k}} \begin{pmatrix} c_{\mathbf{k}\uparrow} \\ c_{\mathbf{k}\downarrow} \end{pmatrix},$$

where

$$h_{\mathbf{k}} = \begin{pmatrix} -\gamma_{\mathbf{k}} - \frac{1}{2} B J_H & -\frac{1}{2} A J_H \\ -\frac{1}{2} A^* J_H & -\gamma_{\mathbf{k}} + \frac{1}{2} B J_H \end{pmatrix}.$$

This 2×2 matrix is easily diagonalized to get the eigenvalues as

$$\lambda_{\mathbf{k}}^{\pm} = \frac{1}{2} (-2\gamma_{\mathbf{k}} \pm J_H \sigma),$$

where $\sigma^2 = \sigma_x^2 + \sigma_y^2 + \sigma_z^2 \equiv |A|^2 + B^2$. The corresponding eigenvectors are

$$|u_{\mathbf{k}}^-\rangle = x_{\mathbf{k}} |\uparrow\rangle + y_{\mathbf{k}} |\downarrow\rangle \quad \text{and} \quad |u_{\mathbf{k}}^+\rangle = y_{\mathbf{k}} |\uparrow\rangle - x_{\mathbf{k}} |\downarrow\rangle,$$

where

$$x_{\mathbf{k}}^2 = \frac{1}{2} \left(1 + \frac{B}{\sigma} \right) \quad \text{and} \quad y_{\mathbf{k}}^2 = \frac{1}{2} \left(1 - \frac{B}{\sigma} \right),$$

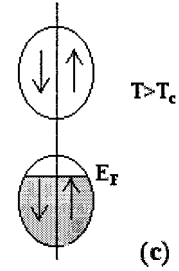
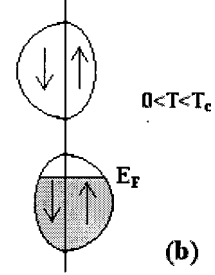
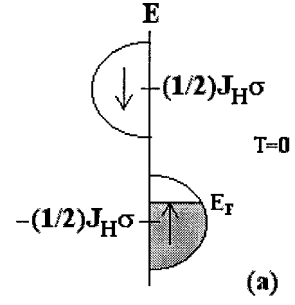


FIG. 2. A schematic diagram of the up and down densities of states at various temperatures: (a) $T=0$, (b) $0 < T < T_c$, and (c) $T \geq T_c$. E_F shows the Fermi energy for the hole doped compound. At finite temperature, the spin eigenstates have a mixed character.

and

$$|\uparrow\rangle = \begin{pmatrix} 1 \\ 0 \end{pmatrix} \quad \text{and} \quad |\downarrow\rangle = \begin{pmatrix} 0 \\ 1 \end{pmatrix}. \quad (10)$$

At zero temperature the t_{2g} spin assumes a saturation value, so $B/\sigma = 1$, and as a result the ground state $|u_{\mathbf{k}}^-\rangle$ has purely up-spin character. The density of states corresponding to $T=0$ is shown schematically in Fig. 2(a). For $T > 0$, $B/\sigma < 1$ and as a result the ground state and excited state have mixed character:

$$N_{\uparrow}(E) = x_{\mathbf{k}}^2 N(E) \quad \text{and} \quad N_{\downarrow}(E) = y_{\mathbf{k}}^2 N(E). \quad (11)$$

The up and down spin characters, $x_{\mathbf{k}}^2$ and $y_{\mathbf{k}}^2$, respectively, are both nonzero in this case, as shown in Fig. 2(b). Finally, for $T \geq T_c$, B vanishes, resulting in $x_{\mathbf{k}}^2 = y_{\mathbf{k}}^2$. This leads to $N(E)$ being an equal admixture of up and down spins¹⁴ as shown schematically in Fig. 2(c). In our theory, the magnetization of the e_g spin is

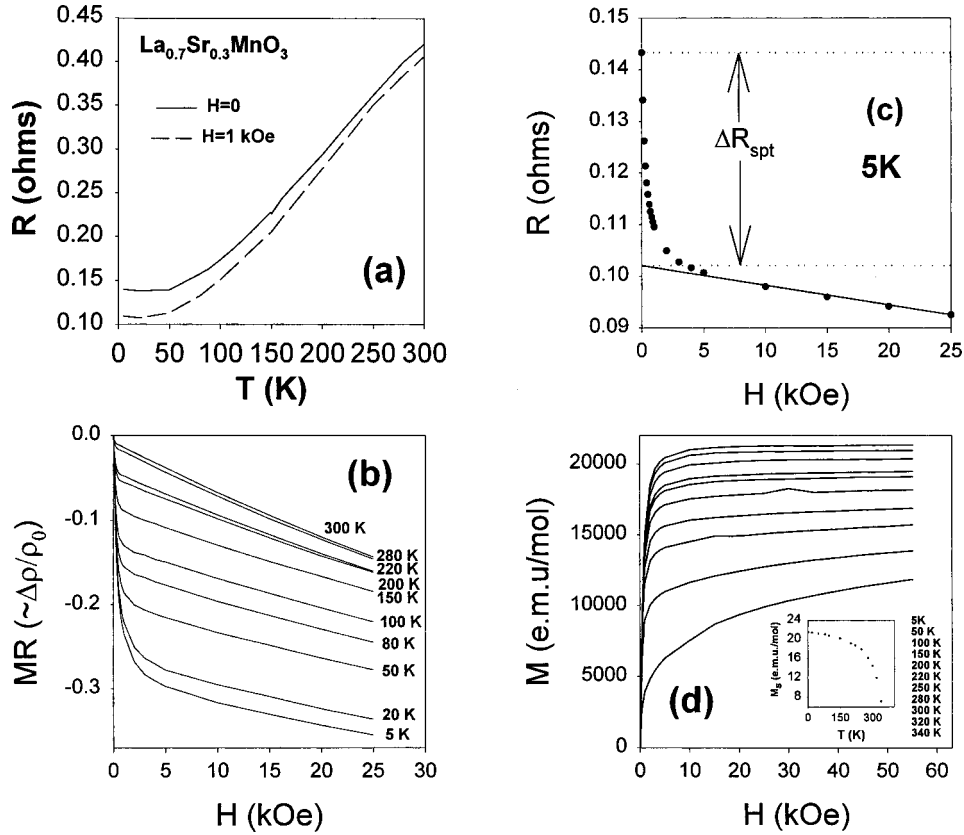


FIG. 3. (a) Resistance versus temperature of $\text{La}_{0.7}\text{Sr}_{0.3}\text{MnO}_3$ from 5 to 300 K in zero field and at 1 kOe where spin-polarized tunneling is the dominant mechanism in magnetoresistance. The magnetoresistance is significant at low temperatures. (b) Magnetoresistance versus field isotherms for polycrystalline $\text{La}_{0.7}\text{Sr}_{0.3}\text{MnO}_3$ from 5 to 300 K. The sharp drop at low fields arises from spin-polarized tunneling at the polycrystalline grain boundaries. (c) The total resistance drop due to spin-polarized tunneling (ΔR_{spt}) is estimated by back extrapolating the linear high-field slope and finding its intercept at zero field. (d) The magnetization versus field isotherms at different temperatures. The inset shows the temperature variation of spontaneous magnetization (M_s) calculated by back extrapolating the linear portion curve after technical saturation. At 340 K the spontaneous magnetization is calculated from the linear portion of the Arrott plot (H/M versus M^2).

$$m_{e_g} = \frac{1}{2}(x_k^2 - y_k^2) = \frac{B}{2\sigma}. \quad (12)$$

Therefore the total (spontaneous) magnetization is $M_s = (B/2\sigma) + B = \alpha B$, where $\alpha = (1 + 1/2\sigma)$. We can thus write x_k^2 and y_k^2 in terms of the reduced magnetization, $m = M_s(T)/M_s(T \rightarrow 0)$ as

$$x_k^2 = (1 + m)/2 \quad \text{and} \quad y_k^2 = (1 - m)/2. \quad (13)$$

Within our theory, the ratio $N_{\uparrow}(E)/N_{\downarrow}(E)$ is independent of energy. Thus, the up and down DOS at the Fermi level, n_{\uparrow} and n_{\downarrow} , which appear in Eqs. (3) and (4) are proportional to x_k^2 and y_k^2 , respectively. Substituting Eq. (13) in the expression for spin-polarized tunneling conductivity in Eqs. (3) and (4), we obtain a relation between ΔR_{spt} and the reduced spontaneous magnetization of the system:

$$\Delta R_{\text{spt}} \propto [1/\sigma(\theta) - 1/\sigma(0)]. \quad (14)$$

Here the conductivity in zero field, $1/\sigma(\theta)$, is averaged over different values of $\cos\theta$ for various grains. While fitting ΔR_{spt} vs m data (see Sec. IV) we have used $\langle \cos(\theta) \rangle$ as a fitting parameter.

III. EXPERIMENT

Bulk samples of $\text{La}_{0.7}\text{Sr}_{0.3}\text{MnO}_3$ were prepared by the wet chemical route. Initially, a stoichiometric mixture of La_2O_3 and Mn was dissolved in nitric acid and $\text{Sr}(\text{NO}_3)_2$ added to it. The cations were coprecipitated as carbonates by adding excess ammonium carbonate to the nitrate solution. This carbonate precursor was then heated at 1200 °C to obtain single-phase $\text{La}_{0.7}\text{Sr}_{0.3}\text{MnO}_3$. The bulk sample of $\text{La}_{0.55}\text{Ho}_{0.15}\text{Sr}_{0.3}\text{MnO}_3$ was prepared by the conventional solid-state reaction route starting from the oxides of La, Ho, and Mn and carbonate Sr. Stoichiometric mixtures of these powders were ground for a few hours in a mortar in acetone base and calcined at 1050 °C for 24 h. The calcined mixture was then reground, pelletized, and sintered at 1450 °C for 30 h and then cooled to room temperature resulting in the single phase. The addition of a small amount of Ho at the La site brings T_c down to 255 K,¹⁵ making it possible to study the spin-polarized tunneling up to T_c in conventional low-temperature cryostats. Electrical measurements were carried out on a rectangular bar shaped sample (2 mm×3 mm×15 mm) using the conventional four-probe technique. Magnetoresistance measurements were made using a homemade superconducting magnet up to fields of 3 T, in the temperature range 5–300 K. Magnetization versus field isotherms were measured on a Quantum Design superconducting quantum

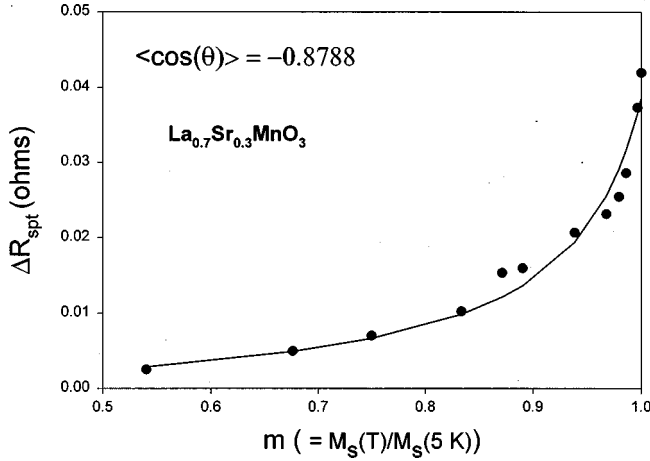


FIG. 4. The total resistance drop due to spin-polarized tunneling (ΔR_{spt}) at different temperatures as a function of the reduced magnetization $m = M_s(T)/M_s(5 \text{ K})$ (filled circles) for $\text{La}_{0.7}\text{Sr}_{0.3}\text{MnO}_3$. The solid line is the theoretical best fit curve [Eq. (14)] to the experimental points. The best fit value of $\langle \cos\theta \rangle$ is -0.8788 .

interference device (SQUID) magnetometer up to a field of 5.5 T.

IV. RESULTS AND DISCUSSION

A. Results on $\text{La}_{0.7}\text{Sr}_{0.3}\text{MnO}_3$

Figure 3(a) shows the resistance versus temperature for $\text{La}_{0.7}\text{Sr}_{0.3}\text{MnO}_3$ in zero field and at an applied field of 1 kOe from 5 to 300 K. There is a significant magnetoresistance at low temperatures at this relatively low field from grain boundary origin. Figure 3(b) shows the magnetoresistance, $\text{MR} \equiv [R(H) - R(0)]/R(0)$, as a function of the applied field (H) from 5 to 300 K. We observe a sharp drop in the MR at low fields and the magnitude of the drop decreases with increasing temperature. This sharp drop is absent in single crystals and epitaxial thin films^{1,2,6} and is therefore associated with the grain boundaries in polycrystalline samples. At high field, the slope of this curve becomes almost linear. The slope increases with increasing temperature and is identical to the nature of the MR vs H curves observed in single crystals. This part of the MR can be ascribed to the Zener double exchange and arises from the intrinsic magnetoresistance of the grains.⁶ To find the total resistance drop associated with the intergranular part (ΔR_{spt}) we extrapolate back the linear high-field region to find its intercept at zero field. This is schematically shown in Fig. 3(c) for the curve obtained at 5 K. Figure 3(d) shows the magnetization versus field (M - H) data for the same sample from 5 to 340 K. The inset shows the spontaneous magnetization (M_s) as a function of temperature calculated by back extrapolating the linear region of the curve beyond technical saturation.

In Fig. 4 we have plotted ΔR_{spt} as a function of $m = M_s(T)/M_s(5 \text{ K})$ along with the theoretical curve [Eq. (14)]. The proportionality constant in Eq. (14) and $\langle \cos\theta \rangle$ are taken as fitting parameters with the implicit assumption that the total density of states at E_F [$n(E_F) = n_{\uparrow} + n_{\downarrow}$] is constant as a function of temperature. This point shall be discussed in detail in the next paragraph. We get the best fit for $\langle \cos\theta \rangle = -0.8788$, which corresponds to $\theta \approx 151.5^\circ$. The negative

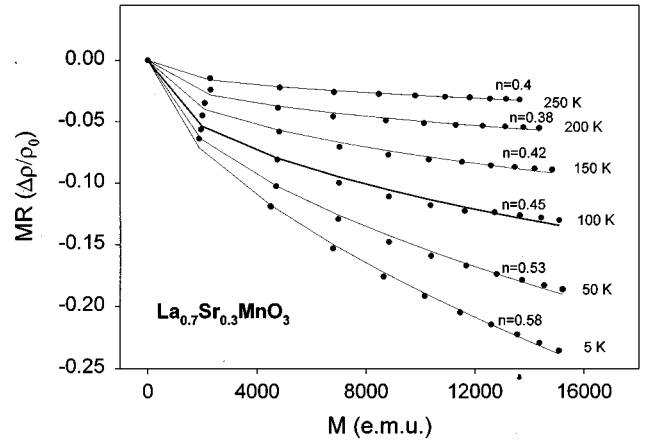


FIG. 5. Magnetoresistance versus magnetization isotherms of $\text{La}_{0.7}\text{Sr}_{0.3}\text{MnO}_3$ at low fields (up to 1 kOe). The solid lines are the best fit to the relation $\text{MR} \propto (M/M_s)^n$. Note that this relation provides a good fit to the data over the entire temperature range.

value of $\langle \cos\theta \rangle$ is consistent with the fact that there are two interactions governing the direction of magnetization of a grain: the easy axis which is random and tends to randomize the direction of the magnetization, and the magnetostatic dipolar interaction between the grains which tend to favor antiparallel alignment between grains.

The assumption that $n(E_F)$ is constant as a function of temperature has to be justified for colossal magnetoresistive materials since many of these materials have a metal-insulator transition (or a transition from a good metal to an incoherent metal¹⁶) at temperatures close to T_c . The temperature evolution of $n(E_F)$ has been recently calculated by Biswas *et al.* from spin-polarized tunneling spectroscopy in a variety of hole doped colossal magnetoresistive manganites.¹⁷ The common feature in all of them is that $n(E_F)$ remains constant up to around $0.8T_c$, above which it drops off rapidly and goes to zero just before T_c . In the case of $\text{La}_{0.7}\text{Sr}_{0.3}\text{MnO}_3$ T_c is around 370 K, which is much above the temperature range in which we have fitted our data.

So far, we have been concerned with the total MR arising from spin-polarized tunneling, that is the total drop in resistance due to spin-polarized tunneling after the technical saturation in magnetization. We now investigate the MR versus M at low fields. This is the regime in which domain rotation takes place, i.e., where $\langle \cos\theta \rangle$ is changing. The MR versus M curves at fields less than 1 kOe are shown in Fig. 5. These curves fit well with a phenomenological power-law behavior: $\text{MR} \propto (M/M_s)^n$, where $n < 1$. However, to fit these curves within our model, we need to compute $\langle \cos\theta \rangle$ as a function of field, and this is beyond the scope of the present work.

B. Results on $\text{La}_{0.55}\text{Ho}_{0.15}\text{Sr}_{0.3}\text{MnO}_3$

Substitution of a smaller size rare-earth Ho at the La site in $\text{La}_{0.7}\text{Sr}_{0.3}\text{MnO}_3$ results in a decrease of the ferromagnetic transition temperature T_c .¹⁵ The T_c for $\text{La}_{0.55}\text{Ho}_{0.15}\text{Sr}_{0.3}\text{MnO}_3$ determined from the maximum in the double derivative of the M - T curve at 5000 Oe [Fig. 6(a)] is 255 K. The system has a metal-insulator transition around the same temperature. Figure 6(b) shows the magnetization

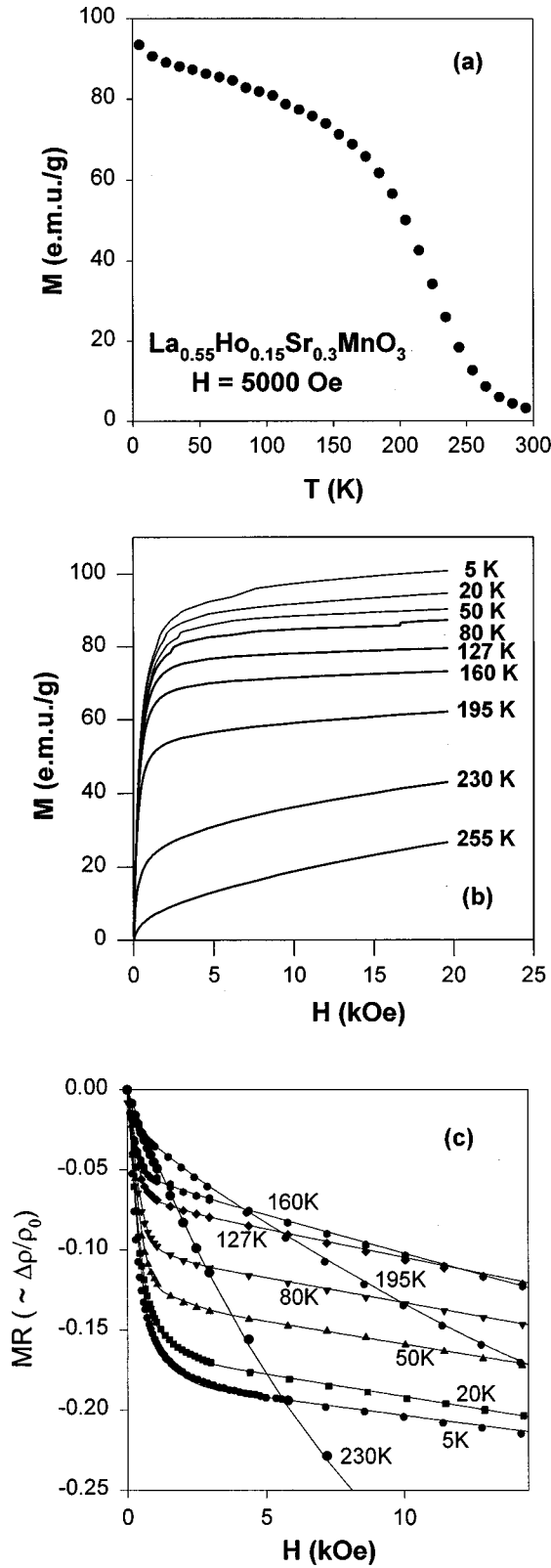


FIG. 6. (a) Magnetization versus temperature of $\text{La}_{0.55}\text{Ho}_{0.15}\text{Sr}_{0.3}\text{MnO}_3$ at 5 kOe. (b) Magnetization versus field up to 20 kOe at various temperatures. (c) Magnetoresistance as a function of field (dots) and the fitted curves (solid lines) using Eq. (15) at various temperatures. The typical values of the parameters at 5 K are $A = -0.2678$, $B = 2.1665$, $C = -0.0125$, $D = 0.4300$, and $J = 2.73 \times 10^{-3}$. The value of K is nonzero only close to T_c .

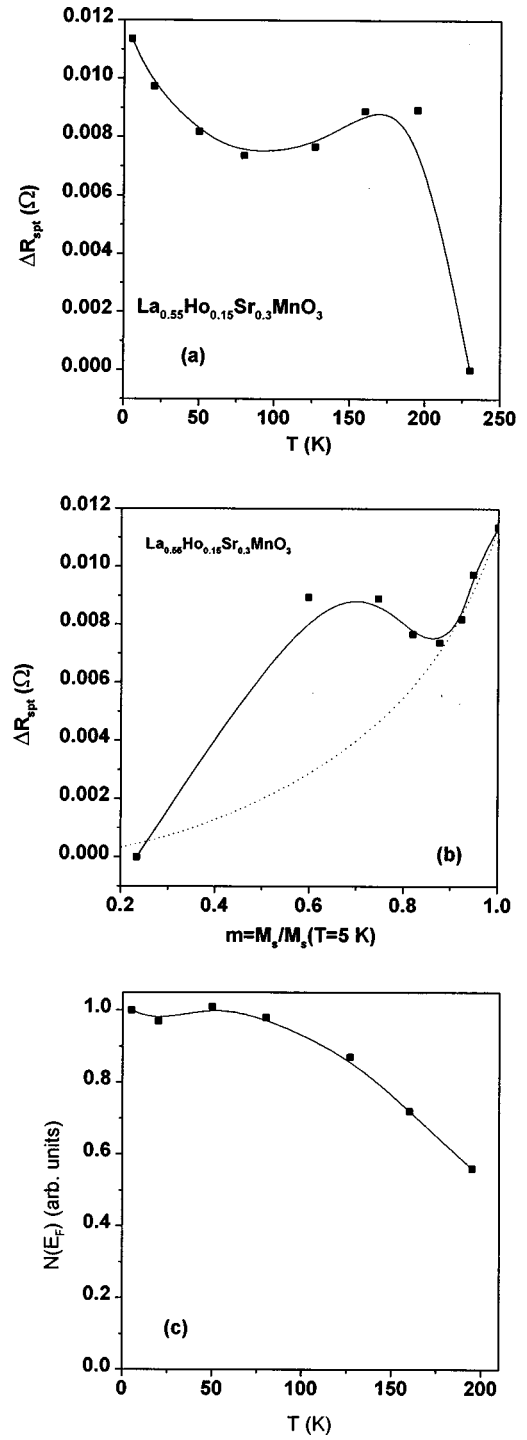


FIG. 7. (a) ΔR_{spt} as a function of temperature from 5 to 230 K; the solid line is a guide to the eye. (b) ΔR_{spt} as a function of the reduced magnetization $m = M_s(T)/M_s(5 \text{ K})$; the dotted line is the theoretical curve for constant $n(E_F)$ using Eq. (14) for $\langle \cos\theta \rangle = -0.63$ and the solid line is a guide to the eye. (c) Temperature variation of $n(E_F)$ derived using Eqs. (3) and (14).

versus field (M - H) at various temperatures below T_c up to a field of 20 kOe. The spontaneous magnetization (M_s) was determined by extrapolating back to zero the linear high-field region of the M - H curve at low temperatures and from the Arrot plot at temperatures close to T_c . Figure 6(c) shows the $\text{MR} (\sim [\rho(H) - \rho(0)]/\rho(0) \sim \Delta\rho/\rho_0)$ versus field at various temperatures. To separate out the contribution due to spin-

polarized tunneling we used a scheme developed earlier.⁶ It was shown that the curve fitted well with an expression of the form

$$\text{MR} = -A \int_0^H f(k) dk - JH - KH^3 \quad \text{with}$$

$$f(k) = A \exp(-Bk^2) + Ck^2 \exp(-Dk^2), \quad (15)$$

where the first term gives the contribution from spin-polarized tunneling and the other two terms give the intrinsic contribution from Zener double exchange. The solid lines in Fig. 6(c) show the fitted curve using this expression. The total resistance drop due to spin-polarized tunneling (ΔR_{spt}) is given by $R_0 A \int_0^H f(k) dk$, where R_0 is the zero-field resistance and the parameters A, B, C, D are taken from the fitted curve at that temperature. One interesting point to note is that we do not observe any contribution to the MR from spin-polarized tunneling in this compound at 230 K though the T_c is around 255 K. The significance of this observation in context of the observations made by Biswas *et al.* will be discussed later. Figure 7(a) shows ΔR_{spt} as a function of temperature. One normally expects this quantity to drop monotonically with temperature due to decreasing polarization of the conduction band. However, at temperatures close to T_c , ΔR_{spt} shows an increase reaching a maximum before dropping to zero. The same feature is observed when ΔR_{spt} is plotted as a function of m [Fig. 7(b)], where ΔR_{spt} does not decrease monotonically as m is reduced but a broad hump is observed.

To understand these results we need to note that in this case we are no longer justified in assuming that $n(E_F)$ is constant over the whole temperature range since the measurements are done at temperatures close to T_c . As discussed earlier $n(E_F)$ drops off rapidly as one approaches T_c . The dotted line in Fig. 7(b) shows the typical ΔR_{spt} as a function of m derived from Eq. (14) with $\langle \cos \theta \rangle \sim -0.63$ when $n(E_F)$ is constant. This curve fits well at low temperatures. However, as discussed in Sec. II it follows from Eq. (3) that ΔR_{spt} is inversely proportional to $\{n(E_F)\}$.² Thus as one approaches T_c , ΔR_{spt} is enhanced due to the decrease in $n(E_F)$.¹⁷ We have attempted to extract the temperature variation of $n(E_F)$ by calculating the quantity $\sqrt{\Delta R_{\text{spt}}^{\text{(theoretical)}} / \Delta R_{\text{spt}}^{\text{(experimental)}}$, where ΔR_{spt} (theoretical) is taken from the computed curve. The calculated quantity is

shown in Fig. 7(c). However, there could be a large error owing to the fact that the range over which the theoretical curve can be fitted is very small. Closer data near T_c would actually be useful to probe the effect of $n(E_F)$ on ΔR_{spt} .

The other interesting feature of this study is the vanishing of ΔR_{spt} at 230 K. It has been shown through tunneling studies¹⁷ in $\text{La}_{0.7}\text{Pb}_{0.3}\text{MnO}_3$ that the DOS at the Fermi level actually drops to zero before T_c . In the vicinity of T_c a gap opens up near E_F . At present the details regarding the nature of this gap are not yet known.

We have thus shown that the model of spin-polarized tunneling proposed in this paper explains well the data on the half metallic ferromagnet $\text{La}_{0.7}\text{Sr}_{0.3}\text{MnO}_3$ and $\text{La}_{0.55}\text{Ho}_{0.15}\text{Sr}_{0.3}\text{MnO}_3$ (with the underlying t_{2g} spins forming a localized magnetic lattice and the e_g spins forming a polarized conduction band). However, Eqs. (3) and (4) should apply equally well to other granular ferromagnetic systems, provided the evolution of the up- and down-spin density of states with temperature is known. It might therefore be also interesting to investigate the nature of spin-polarized tunneling in more conventional granular itinerant ferromagnets within the realms of this model.

V. CONCLUSION

In summary, we have developed a mean-field model for spin-polarized tunneling in granular itinerant ferromagnets. The theoretical model provides a satisfactory fit for our data on the temperature dependence of the magnetoresistance due to spin-polarized tunneling in the half metallic ferromagnet $\text{La}_{0.7}\text{Sr}_{0.3}\text{MnO}_3$. It also explains the evolution of the magnetoresistance due to spin-polarized tunneling in $\text{La}_{0.55}\text{Ho}_{0.15}\text{Sr}_{0.3}\text{MnO}_3$ when the temperature dependence of the total density states is taken into account. Further investigations on other systems should provide a better understanding of the transport mechanism in itinerant magnetic systems.

ACKNOWLEDGMENTS

We would like to thank K. V. Gopalakrishnan for his help regarding SQUID measurements and Arun Paramekanti, Praveen Chaddah, and S. Ramakrishnan for useful discussions. We would also like to thank R. S. Sannabhadhi and Arun Patade for technical help.

*Electronic address: prat@tifr.res.in

[†]Permanent address: Indian Institute of Technology, Kharagpur, India.

¹H. Y. Hwang, S.-W. Cheong, N. P. Ong, and B. Batlogg, Phys. Rev. Lett. **77**, 2041 (1996).

²X. W. Li, A. Gupta, Gang Xiao, W. Qian, and V. P. Dravid, Appl. Phys. Lett. **71**, 1124 (1997).

³S. Sundar Manoharan, D. Elephant, G. Reiss, and J. B. Goodenough, Appl. Phys. Lett. **72**, 984 (1998).

⁴J. M. D. Coey, A. E. Berkowitz, Ll. Balcells, F. F. Putris, and F. T. Parker, Appl. Phys. Lett. **72**, 734 (1998).

⁵J. M. D. Coey, A. E. Berkowitz, Ll. Balcells, F. F. Putris, and A.

Barry, Phys. Rev. Lett. **80**, 3815 (1998).

⁶P. Raychaudhuri, T. K. Nath, A. K. Nigam, and R. Pinto, J. Appl. Phys. **84**, 2048 (1998).

⁷R. Shreekala, M. Rajeswari, K. Ghosh, A. Goyal, J. Y. Gu, C. Kwon, Z. Trajanovic, T. Boettcher, R. L. Greene, R. Ramesh, and T. Venkatesan, Appl. Phys. Lett. **71**, 282 (1997).

⁸C. Zener, Phys. Rev. **82**, 403 (1951).

⁹J. S. Helman and B. Abeles, Phys. Rev. Lett. **37**, 1429 (1976).

¹⁰J. Inoue and S. Maekawa, Phys. Rev. B **53**, R11 927 (1996).

¹¹N. Furukawa, J. Phys. Soc. Jpn. **64**, 3164 (1995).

¹²N. Furukawa, J. Phys. Soc. Jpn. **64**, 2754 (1995).

¹³N. Furukawa, J. Phys. Soc. Jpn. **64**, 2734 (1995).

- ¹⁴N. Furukawa has solved the ferromagnetic Kondo Hamiltonian with strong Hund's rule coupling in infinite dimension using dynamical mean-field theory. Our approach using a simple mean-field theory gives qualitatively the same evolution of the DOS as that obtained by Furukawa (see, for example, Ref. 11).
- ¹⁵P. Raychaudhuri, T. K. Nath, P. Sinha, C. Mitra, A. K. Nigam, S. K. Dhar, and R. Pinto, *J. Phys.: Condens. Matter* **9**, 10 919 (1997).
- ¹⁶Nobuo Furukawa, Yutaka Moritomo, K. Hirota, and Y. Endoh, cond-mat/9808076 (unpublished).
- ¹⁷Amlan Biswas, Suja Elizabeth, A. K. Raychaudhuri, and H. L. Bhat, *Phys. Rev. B* **59**, 5368 (1999).